Preprints of the 19th World Congress
The International Federation of Automatic Control
Cape Town, South Africa. August 24-29, 2014

Robustness Comparison of Battery State of Charge Observers for Automotive Applications ⋆

Björn Fridholm * **Magnus Nilsson** * **Torsten Wik** **

* *Viktoria Swedish ICT, Göteborg, Sweden (e-mail: bjorn.fridholm@viktoria.se, magnus.nilsson@viktoria.se).*
** *Automatic Control, Dept. of Signals and Systems, Chalmers University of Technology, Göteborg, Sweden (e-mail: torsten.wik@chalmers.se)*

Abstract:
This paper compares the robustness of three different battery State of Charge (SoC) estimation algorithms: the Extended Kalman Filter (EKF), the Unscented Kalman Filter (UKF) and the H_∞ filter. Their performance when subject to disturbances such as parameter uncertainties, different sensor noise characteristics and sensitivity to tuning of the filter are examined.
Simulations show that the appropriate choice of observer algorithm will depend on battery chemistry as well as on the intended application. For batteries with a strong correlation between SoC and OCV, the UKF is robust to disturbances such as sensor bias. The H_∞ observer shows performance on par with the UKF but the variability of the estimation errors are larger. The EKF is a good all-round choice.

Keywords: State estimation; Kalman filters; Robustness; H-infinity; Automotive; Hybrid vehicles

1. INTRODUCTION

To secure safety, reliability and performance of an electrified vehicle, it is important to monitor the State of Charge (SoC) of the battery system [Lu et al., 2013]. Batteries are electrochemical components and there are currently no sensors that can measure SoC directly. Instead, electrical signals, such as current and voltages of the battery are used to estimate the SoC via some algorithm. There are several approaches to model based SoC estimation available in literature, such as the Extended Kalman Filter (EKF) [Plett, 2004], the Unscented Kalman Filter (UKF) [Plett, 2006], Luenberger Observers (LO) [Hu et al., 2010], Sliding Mode Observers (SMO) [Kim, 2006] and H_∞ observers [Yan et al., 2010].

There are also several types of Li-Ion batteries in production today. These differ in electrode materials, leading to different electrical behaviour when subject to a charging or discharging current. Due to these differences, the model used in the observers are not necessarily the same for different cell chemistries [Hu et al, 2012a].

Another aspect to consider when evaluating SoC estimators is that the battery usage is different depending on vehicle application. In a Battery Electric Vehicle (BEV), the battery is the only energy source and thus a large part of the SoC range will be used. In a Hybrid Electric Vehicle (HEV), the electric system is mainly used to boost power in accelerations and thus the battery will be designed to handle large charge and discharge power, but the used SoC range is normally rather small. A Plug-In Hybrid Electric Vehicle (PHEV) can be used as either a BEV or HEV or any combination in between.

Comparative studies of SoC estimators have been performed before, [Li et al., 2013] compare EKF, UKF and LO while [Chen et al., 2012] focus on LO compared to SMO. The main focus in those papers are on the algorithms and implementation aspects of the observers. In [Hu et al., 2012b], the robustness of an EKF is analysed with respect to temperature and ageing for two different battery types. However, there has been no thorough comparison of the performance of different observers for different battery chemistries.

This paper compares the performance of the EKF to that of the UKF and the H_∞ filter for two different battery chemistries. Using a Monte Carlo simulation approach, robustness to problems such as parameter uncertainties, sensor noise characteristics and observer tuning is analysed. The choice of observers is based on promising results shown in [Plett, 2004], [Plett, 2006] and [Yan et al., 2010]. These observers can also be implemented by simple and efficient recursive algorithms. In [Kim, 2006], Kim show the potential of the SMO. The implementation is, however, complex compared to the chosen observers, and it is thus left out of the evaluation.

The paper is structured as follows: Section 2 presents the test environment used in the evaluation with battery model, observers and the considered use cases. In Section 3, the robustness evaluation is presented. In Section 4

⋆ This work was supported by the Swedish Energy Agency.

some conclusions of the tests are drawn and the results are discussed.

2. EXPERIMENT SETUP

This section describes the test setup used, i.e. the simulation environment consisting of battery and sensor models and the evaluated observers. Also the drive cycles used in the tests are presented, together with metrics to evaluate the observers.

2.1 Battery Model

The observers evaluated are all model based and require a model of the process. The general nonlinear discrete time state space form

$$\begin{aligned} x_{k+1} &= f(x_k, u_k, w_k) \\ y_k &= h(x_k, u_k, v_k) \\ w_k &\sim \mathcal{N}(\bar{w}_k, \Sigma_{w,k}) \\ v_k &\sim \mathcal{N}(\bar{v}_k, \Sigma_{v,k}) \end{aligned} \tag{1}$$

is used, where $\mathcal{N}(\bar{\nu}, \Sigma)$ denotes normally distributed noise with mean $\bar{\nu}$ and variance Σ.

Two different batteries are considered in the study; one lithium iron phosphate (LFP) and one lithium nickel manganese cobalt oxide (NMC). Equivalent circuit models, see Figure 1, were fitted to lab data for both batteries. While it was concluded that both batteries can be suitably modelled by single RC-circuit models, the LFP battery needed a hysteresis state, u_h, to improve the fit to measured data.

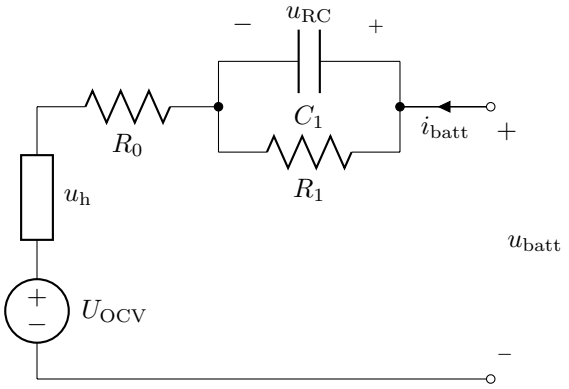

Fig. 1. Equivalent circuit battery model

The model equations for both batteries are given in the following sections. For further descriptions of the models, see [Hu et al, 2012a] and [Plett, 2004].

NMC In room temperature, the NMC battery can be modelled with sufficient accuracy using the following model:

$$\begin{cases} u_{\mathrm{RC},k+1} = e^{-\frac{\Delta t}{\tau_{1,k}}} u_{\mathrm{RC},k} + R_{1,k}\left(1 - e^{-\frac{\Delta t}{\tau_{1,k}}}\right) i_{\mathrm{batt},k} \\ z_{k+1} = z_k + \dfrac{\eta_i \Delta t}{C_\mathrm{n}} i_{\mathrm{batt},k} \end{cases}$$
$$u_{\mathrm{batt},k} = U_\mathrm{OCV}(z_k) + u_{\mathrm{RC},k} + R_0(z_k) i_{\mathrm{batt},k}$$

Here, u_RC, R_1 and $\tau_1 = R_1 C_1$ are the voltage, resistance and time constant of the RC network, Δt is the sampling time, i_batt and u_batt are battery current and voltage, z is the battery SoC, η_i is the Coulombic efficiency, C_n is the nominal capacity of the battery, U_OCV is the open circuit voltage and R_0 is the internal resistance of the battery. Note that the circuit parameters are varying with SoC, i.e. τ_1, R_1, R_0 and U_OCV are all functions of SoC.

LFP The LFP battery needs an additional hysteresis state. The model used is

$$\begin{cases} u_{\mathrm{RC},k+1} = e^{-\frac{\Delta t}{\tau_{1,k}}} u_{\mathrm{RC},k} + R_{1,k}\left(1 - e^{-\frac{\Delta t}{\tau_{1,k}}}\right) i_{\mathrm{batt},k} \\ u_{\mathrm{h},k+1} = e^{-\kappa_k \Delta t} u_{\mathrm{h},k} + \left(1 - e^{-\kappa_k \Delta t}\right) U_{\mathrm{h,max}}(z_k) \\ z_{k+1} = z_k + \dfrac{\eta_i \Delta t}{C_\mathrm{n}} i_{\mathrm{batt},k} \end{cases}$$
$$u_{\mathrm{batt},k} = U_\mathrm{OCV}(z_k) + u_{\mathrm{RC},k} + u_{h,k} + R_0(z_k) i_{\mathrm{batt},k}$$

where u_h is the hysteresis voltage, κ is the time constant of the hysteresis which is a function of the battery current and $U_\mathrm{h,max}$ is the maximum hysteresis. For the LFP battery, also variations with respect to current and charge/discharge are needed, and thus τ_k and R_1 are functions of battery current as well as SoC.

2.2 State of Charge Observers

Three SoC observers were implemented, sharing battery model and parameters according to Section 2.1.

Extended Kalman Filter The EKF treats the nonlinearities by linearizing the state space representation (1) at each time step. It is a two-step procedure where the *a priori* state and covariance estimates, $\hat{x}^-$ and $\Sigma_{\tilde{x}}^-$, are first calculated using the state space model. Based on the predicted and measured system output, the estimates are then corrected by the *Kalman gain* K to form the *a posteriori* estimate, $\hat{x}^+$ and $\Sigma_{\tilde{x}}^+$.

A recursive algorithm suited for real-time implementation is described by

$$\begin{aligned} \hat{x}_k^- &= f\left(\hat{x}_{k-1}^+, u_{k-1}, \bar{w}_{k-1}\right) \\ \Sigma_{\tilde{x},k}^- &= \hat{A}_{k-1} \Sigma_{\tilde{x},k-1}^+ \hat{A}_{k-1}^T + \hat{W}_{k-1} \Sigma_{w,k} \hat{W}_{k-1}^T \\ \hat{y}_k &= h\left(\hat{x}_k^-, u_k, \bar{v}_k\right) \\ K_k &= \Sigma_{\tilde{x},k}^- \hat{C}_k^T \left[\hat{C}_k \Sigma_{\tilde{x},k}^- \hat{C}_k^T + \hat{V}_k \Sigma_{v,k} \hat{V}_k^T\right]^{-1} \\ \hat{x}_k^+ &= \hat{x}_k^- + K_k\left(y_k - \hat{y}_k\right) \\ \Sigma_{\tilde{x},k}^+ &= \left(I - K_k \hat{C}_k\right) \Sigma_{\tilde{x},k}^- \end{aligned} \tag{2}$$

where $\hat{A}_k$, $\hat{W}_k$, $\hat{C}_k$ and $\hat{V}_k$ are the Jacobians:

$$\begin{aligned} \hat{A}_k &= \frac{\partial f(x_k, u_k, w_k)}{\partial x_k}\Big|_{x_k = \hat{x}_k^+} \\ \hat{W}_k &= \frac{\partial f(x_k, u_k, w_k)}{\partial w_k}\Big|_{w_k = \bar{w}_k} \\ \hat{C}_k &= \frac{\partial h(x_k, u_k, v_k)}{\partial x_k}\Big|_{x_k = \hat{x}_k^-} \\ \hat{V}_k &= \frac{\partial h(x_k, u_k, v_k)}{\partial v_k}\Big|_{v_k = \bar{v}_k} \end{aligned}$$

Note that in (2), the Jacobians $\hat{A}_{k-1}$ and $\hat{W}_{k-1}$ from the previous time step are used. For more information on how to derive the EKF, the user is referred to e.g. [Plett, 2004], [Simon, 2006] and [Welch and Bishop, 1995].

Unscented Kalman Filter The UKF uses a similar predict/correct procedure as the EKF, but rather than using the Jacobians to linearize the system, the UKF lets several perturbed versions of the current state vector, called sigma points, pass the nonlinear system (1). The estimated state is calculated as a weighted mean of the result, in general providing a better approximation for strong nonlinearities [Simon, 2006].

The recursive algorithm is more complex than the EKF. First, define the augmented state and sigma point vectors

$$x_k^a = \left[x_k^T, w_k^T, v_k^T\right]^T$$
$$\chi_k^a = \left[\left(\chi_k^x\right)^T, \left(\chi_k^w\right)^T, \left(\chi_k^v\right)^T\right]^T$$

State and covariance estimate predictions are given by

$$\chi_{k-1}^{a,+} = \left\{\hat{x}_{k-1}^{a,+}, \hat{x}_{k-1}^{a,+} + \gamma\sqrt{\Sigma_{\tilde{x},k-1}^{a,+}}, \hat{x}_{k-1}^{a,+} - \gamma\sqrt{\Sigma_{\tilde{x},k-1}^{a,+}}\right\}$$
$$\chi_{k,i}^{x,-} = f\left(\chi_{k-1,i}^{x,+}, u_{k-1}, \chi_{k-1,i}^{w,+}\right)$$
$$\hat{x}_k^- = \sum_{i=0}^{p} \alpha_i^{(m)} \chi_{k,i}^{x,-}$$
$$\Sigma_{\tilde{x},k}^- = \sum_{i=0}^{p} \alpha_i^{(c)} \left(\chi_{k,i}^{x,-} - \hat{x}_k^-\right)\left(\chi_{k,i}^{x,-} - \hat{x}_k^-\right)^T$$

An estimate of the output is calculated from the predicted state

$$\mathcal{Y}_{k,i} = h\left(\chi_{k,i}^{x,-}, u_k, \chi_{k-1,i}^{v,+}\right)$$
$$\hat{y}_k = \sum_{i=0}^{p} \alpha_i^{(m)} \mathcal{Y}_{k,i}$$

The gain of the estimator is

$$\Sigma_{\tilde{y},k} = \sum_{i=0}^{p} \alpha_i^{(c)} \left(\mathcal{Y}_{k,i} - \hat{y}_k\right)\left(\mathcal{Y}_{k,i} - \hat{y}_k\right)^T$$
$$\Sigma_{\tilde{x}\tilde{y},k}^- = \sum_{i=0}^{p} \alpha_i^{(c)} \left(\chi_{k,i}^{x,-} - \hat{x}_k^-\right)\left(\mathcal{Y}_{k,i} - \hat{y}_k\right)^T$$
$$K_k = \Sigma_{\tilde{x}\tilde{y},k}^- \Sigma_{\tilde{y},k}^{-1}$$

Finally, the state and covariance estimates are corrected according to

$$\hat{x}_k^+ = \hat{x}_k^- + K_k\left(y_k - \hat{y}_k\right)$$
$$\Sigma_{\tilde{x},k}^+ = \Sigma_{\tilde{x},k}^- - K_k \Sigma_{\tilde{y},k} K_k^T$$

A thorough background to the unscented transformation and derivation of the UKF can be found in [Simon, 2006] and [Plett, 2006].

Extended H_∞ Filter H_∞ filters have close similarities to Kalman filters, as pointed out by [Simon, 2006]. They are just like Kalman filters for linear systems, but can also be used for nonlinear systems by extended [Seo et al., 2005] and unscented [Ni , 2011] transformations. In the SoC estimation field, [Yan et al., 2010] promotes the use of the H_∞ filter, based on the fact that it does not require information on noise characteristics.

In [Hassibi et al., 1996], the sub-optimal H_∞ filtering problem is formulated as that of finding an estimate $\hat{x}$ such that

$$\sup_{x_0, w\in H_2, v\in H_2} = \frac{\|L_k x_k - L_k \hat{x}_k\|_2^2}{\|x_0 - \hat{x}_0\|_{P_0^{-1}}^2 + \|w_k\|_2^2 + \|v_k\|_2^2} < \gamma^2 \quad (3)$$

for some predefined error bound γ and state weight matrix L. A solution to the problem is given by the recursion

$$\hat{x}_k^- = f\left(\hat{x}_{k-1}^+, u_{k-1}, \bar{w}_{k-1}\right)$$
$$R_k = \begin{bmatrix} I & 0 \\ 0 & -\gamma^2 I \end{bmatrix} + \begin{bmatrix} \hat{C}_k \\ L_k \end{bmatrix} P_{k-1} \begin{bmatrix} \hat{C}_k^T L_k^T \end{bmatrix}$$
$$P_k = \hat{A}_k P_{k-1} \hat{A}_k^T + \hat{W}_k \hat{W}_k^T - \hat{A}_k P_{k-1} \begin{bmatrix} \hat{C}_k^T & L_k^T \end{bmatrix} R_k^{-1} \begin{bmatrix} \hat{C}_k \\ L_k \end{bmatrix} P_{k-1} \hat{A}_k^T$$
$$K_k = P_k \hat{C}_k^T \left[\hat{V}_k \hat{V}_k^T + \hat{C}_k P_k \hat{C}_k^T\right]^{-1}$$
$$\hat{x}_k^+ = \hat{x}_k^- + K_k\left(y_k - h\left(\hat{x}_k^-, u_k, \bar{v}_k\right)\right)$$

For the solution to actually solve the sub-optimal H_∞ filtering problem, the following condition must also hold:

$$P_k^{-1} + \hat{C}_k^T \hat{C}_k - \gamma^{-2} L_k^T L_k > 0 \quad (4)$$

2.3 Filter Tuning

The H_∞ filter is not relying on the noise covariance estimates, Σ_w and Σ_v. The only parameters chosen by the user is the state weight matrix L and error bound γ. They must be chosen such that (4) is fulfilled, but otherwise the estimate is rather insensitive to tuning, as will be shown later in Section 3.

The performance of the EKF and UKF observers depend on the tuning of the covariance matrices Σ_w and Σ_v. To make a fair comparison, an automatic procedure for tuning the covariance matrices was implemented. The procedure, presented by [Abbeel et al., 2005], uses information from an improved set of measurements, y^*, compared to the final application. Here, it is assumed that the improved output has a linear relation to the state, i.e. $y^* = Hx$. The prediction likelihood is maximized by solving the optimization problem

$$\langle \Sigma_w, \Sigma_v \rangle = \arg\max_{\Sigma_w, \Sigma_v} \sum_{k=0}^{N} -\log|2\pi\Omega_k| - \tilde{y}_k^{*T} \Omega_k^{-1} \tilde{y}_k^* \quad (5)$$

with $\Omega_k = H_k \Sigma_{\tilde{x},k} H_k^T + \Sigma_{y^*}$, where Σ_{y^*} is the variance of the improved measurement, N is the number of samples in the test and $\tilde{y}_k^* = (y_k^* - \hat{y}_k)$.

This work is simulation based, and thus the true SoC is available to use as y^*. For the u_{RC} and u_{h} voltages, no individual measurements are available. However, they are related to the SoC via circuit parameters and the output equation, so it is possible to get an estimate of the complete covariance matrix.

Having only the SoC as y^*, (5) can be simplified. First note that $H_k = 1$ in this case and secondly that Σ_{y^*} was assumed small compared to the variance of the SoC estimate $\Sigma_{\hat{z}}$, and was discarded. The optimization problem (5) then simplifies to the scalar expression

$$\langle \Sigma_w, \Sigma_v \rangle = \arg\max_{\Sigma_w, \Sigma_v} \sum_{k=0}^{N} -\log|2\pi\Sigma_{\hat{z},k}| - \frac{(y_k^* - \hat{z}_k)^2}{\Sigma_{\hat{z},k}}$$

which was solved using a simple search algorithm presented in [Abbeel et al., 2005].

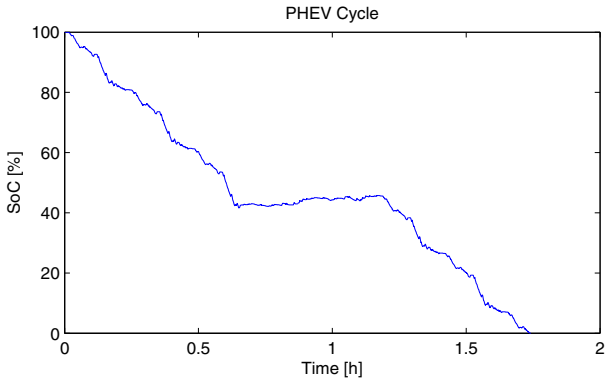

(a) PHEV

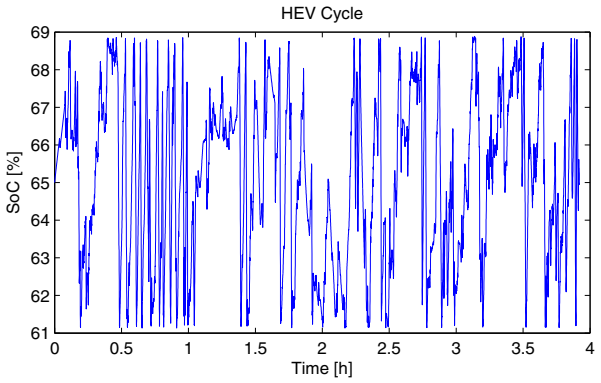

(b) HEV

Fig. 2. Drive cycles for the PHEV and HEV use case, note the different scaling of the y-axis

The two main difficulties found using the method were:

- The result is sensitive to initial estimates. This was overcome by using several different initial estimates.
- The improved SoC signal uses Coulomb counting, as do the estimators. In order to find a trade-off between Coulomb counting and the information from the measured cell voltage, an initial SoC estimation error was needed.

2.4 Use Cases

Depending on the level of electrification of the target vehicle, the use of the battery will be different. An HEV using only a small part of the SoC range will have fewer possibilities to calibrate the estimation, while a PHEV or BEV must handle larger SoC ranges and may also need higher precision in their estimates. In the evaluation, two cycles were used, see Figure 2. One for HEV where the SoC swing is approximately 10 % and one PHEV cycle starting from a fully charged battery and then slowly draining it to empty with a charge sustaining part in the middle. BEV is considered to be similar to PHEV with the exception of the charge sustaining portion of the cycle and thus no additional cycle was added for this case.

2.5 Performance Indicators

In order to assess the performance of the different observers, a set of metrics is needed. The evaluations are based on 100 Monte Carlo simulations and the performance indicators used must give a representative value over all these simulations. In [Li et al., 2001], several aspects of the choice of performance indicators are discussed. In this evaluation, the following were selected:

Mean Absolute Percentage Error The average error in percent was considered an appropriate measure since it has a direct interpretation. The MAPE is given by

$$\text{MAPE} = \frac{1}{MN}\sum_{j=1}^{M}\sum_{i=1}^{N}|\tilde{z}_{i,j}|$$

where M is the number of Monte Carlo simulations, N is the number of samples in one simulation and $\tilde{z} = z - \hat{z}$ is the SoC error in percent.

Max Percentage Error The max error gives an important worst case measure. It is taken over all simulations according to

$$\text{MAX} = \max_{i,j}|\tilde{z}_{i,j}|$$

Note that the first n samples of each simulation is left out in order to reduce the influence of the initial error. In this work, $n = 1000$ seconds was used.

2.6 Limitations

There are some limitations imposed on the test setup and evaluation.

Tuning To reduce the time needed for tuning of the observers, the procedure presented in Section 2.3 is used to optimize the covariance matrix over the whole SoC range. Improved estimates may be achieved using matrices that depend on SoC. The same tuning is also used for both the HEV and PHEV cycles.

Unmodelled Behaviour The performance of the observers is highly dependent on the quality of the model used. To minimize the influence of unmodelled behaviour in the evaluation, the same model is used to provide the reference SoC as is used in the observers.

3. ROBUSTNESS ANALYSIS

This section presents the different test cases and the results of the robustness evaluation.

3.1 Benchmark Test

The first test uses correct model and observer parameters and only adds Gaussian noise on the current and voltage sensors. Also, based on this noise, an initial SoC error is imposed on the observers. The results from this test provide an indication on the best performance that can be expected from each observer type.

In Figure 3 the results of 100 Monte Carlo simulations are plotted. It can be seen that the errors are small in almost all cases. Only the UKF for the LFP battery has trouble finding the correct SoC due to the flat OCV curve, see Figure 4a. Note that the tuning used is a compromise between the HEV and PHEV cycles. The UKF can be tuned to produce slightly better estimates for HEV, but that negatively impacts the performance for PHEV case.

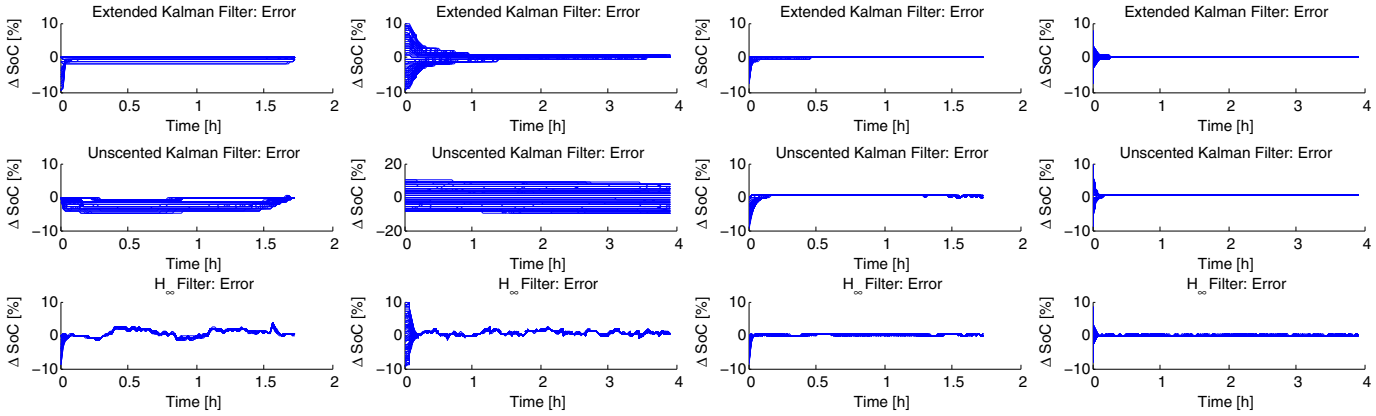

(a) LFP, PHEV (b) LFP, HEV (c) NMC, PHEV (d) NMC, HEV

Fig. 3. Benchmark simulation only adding Gaussian noise with small variance to current and voltage sensor values. Most simulated cases are acceptable from a SoC accuracy perspective, but the UKF estimate for the LFP battery on the HEV cycle shows an almost constant offset depending on the initial estimation error.

3.2 Model Parameter Uncertainties

The characteristics of a battery depends on several factors, e.g. SoC, temperature and age. Even if the battery model parameters are calibrated on-line, the algorithm must be robust to deviations from optimal parameters in the model. In the evaluation, the reasons for a deviation in parameter values are not considered. Instead, it is the algorithms' ability to handle the erroneous model parameters that is in focus. The parameters of the battery model used in the observers were randomly distorted from the values used in the reference model. Gaussian noise was also added to the measurement signals as in the benchmark test.

For the analysis, the case where the OCV is uncertain was separated from the other parameter variations since the impact of an erroneous OCV can be severe.

OCV Errors In Figure 4, the OCV curves of the two batteries are shown. The OCV robustness tests evaluate how the observers handle perturbations of magnitudes up to 0.01V compared to the nominal OCV curve.

In Figure 5, the results of 100 Monte Carlo simulations are shown for all four combinations of battery and use case. In general, the impact of an uncertain OCV curve is most severe for the NMC battery. The reason for this is that the observers use the OCV curve more for the NMC battery compared to the LFP battery. For the NMC battery all three estimators show similar results, both for HEV and PHEV cycles. For the LFP battery the UKF have trouble converging with a more or less constant estimation error for most part of the SoC range. The impact of this is most severe on the HEV cycle. The estimation error of the H_∞ filter is varying a lot during the cycle, but the convergence rate is fast also for the combination of LFP battery and HEV cycle, which is the most difficult combination.

Parameter Errors The parameters of the battery model used by the observer will vary with SoC, temperature, age, etc. This test is designed to examine the ability of the respective observer to handle uncertainties in the

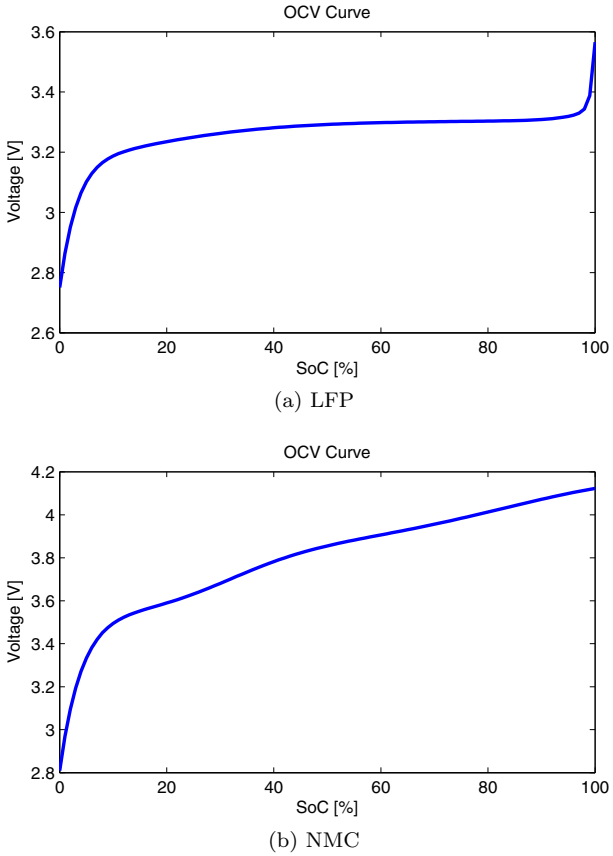

(a) LFP

(b) NMC

Fig. 4. OCV curve of the evaluated batteries

model parameters. Random perturbations are added to the resistances R_0 and R_1, to the time constant τ_1 and to the capacity of the battery C_n. The worst-case errors are rather large in order to push the observers to the limits of what they can handle. The results of the simulations are shown in Figure 6.

The H_∞ observer is most sensitive to errors in model parameters for both batteries. The differences between observers are, however, rather small for all but the PHEV cycle with the LFP battery.

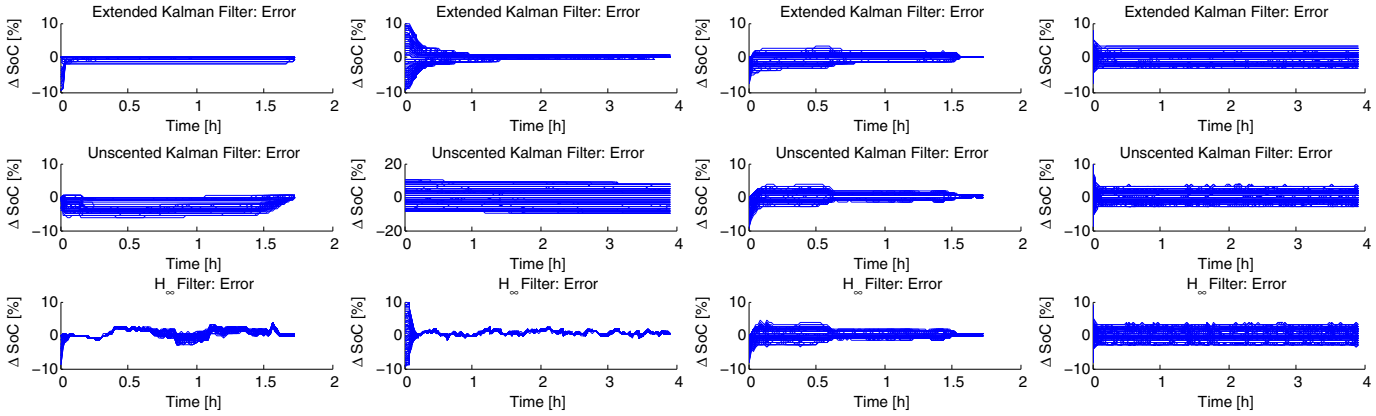

(a) LFP, PHEV (b) LFP, HEV (c) NMC, PHEV (d) NMC, HEV

Fig. 5. Results from Monte Carlo simulations for with perturbations of OCV curve

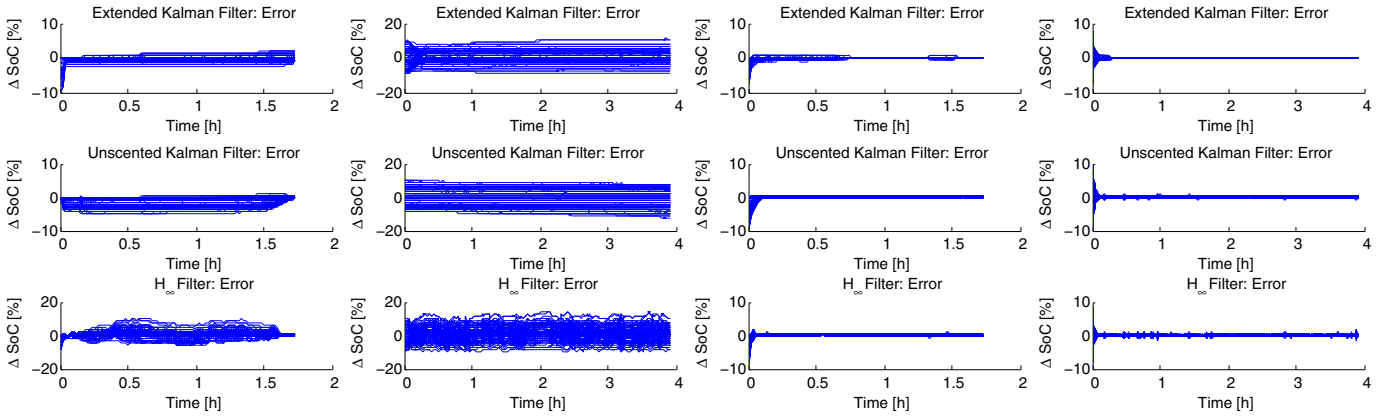

(a) LFP, PHEV (b) LFP, HEV (c) NMC, PHEV (d) NMC, HEV

Fig. 6. Results from Monte Carlo simulations with perturbations of model parameters.

3.3 Sensor Noise

Gaussian noise is added to the sensors in all the tests in this evaluation. Two tests were specifically designed to evaluate the robustness to erroneous assumptions of noise characteristics, one adding bias to the current sensor estimate and the other increasing the variance of the voltage measurement.

Current Sensor Bias In this test, the bias of the current sensor is chosen as a normally distributed random variable with variance chosen to give a maximum deviation over the realizations of approximately 1A. The results are shown in Figure 7. For the LFP battery, the H_∞ filter shows no drift of the estimation. However, just as in all other cases, the variability of the estimates are large. The EKF performance is on par with H_∞ for the whole cycle, but is also constantly drifting which means that it is not suitable for a long-term drive with biased current sensor. The UKF also shows drift and is further set back by its poor performance for the LFP battery. When the OCV curve provides the observer with more information, like in the case of the NMC battery, the UKF handles the bias well for both the HEV and PHEV cycles. We may also note that the H_∞ estimate is slightly better than the EKF estimate for the NMC battery.

Voltage Sensor Variance In this test, the variance of the voltage sensor is varied. The standard deviation of the voltage sensor used in the simulations are 0.1-1mV, compared to 0.3mV used in the other simulations. The main observation in this test is the poor performance of the H_∞ filter, particularly for the NMC battery, see Figure 8. This makes the H_∞ filter less suited if the uncertainty of the voltage measurement is large. This result can seem surprising, given that the H_∞ filter does not use any information on the noise characteristics of the measurement signals. For this reason, it is easy to assume that it is robust to differences in variance. However, a closer study of the robustness bound (3) using the actual values for L and γ, gives a bound that is actually larger than the full SoC range.

3.4 Sensitivity to Observer Tuning

The EKF and UKF have covariance matrix parameters, Σ_w and Σ_v, that must be tuned. Tuning is expensive and in real world applications it is not feasible to expect that an optimal set of observer parameters is used. For this

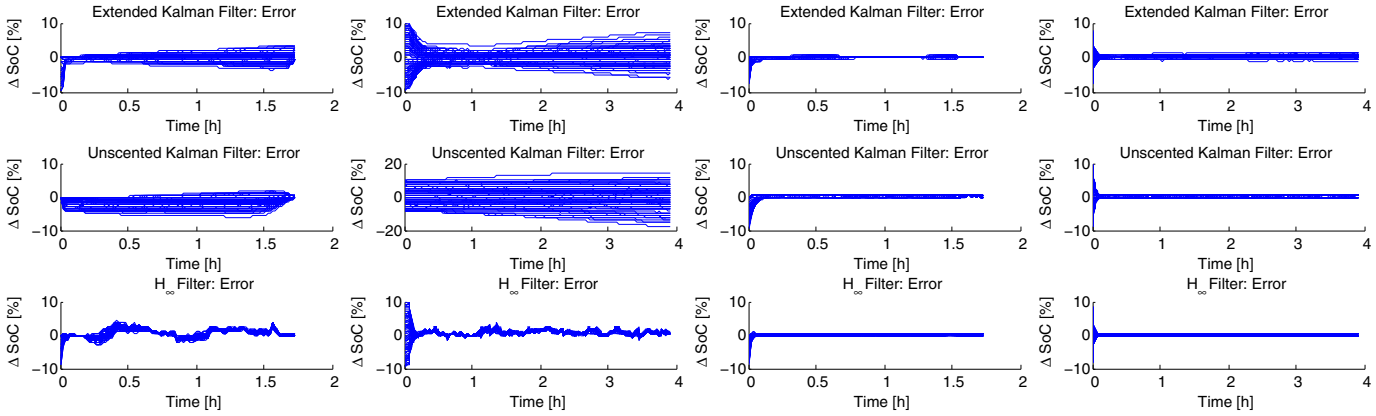

(a) LFP, PHEV (b) LFP, HEV (c) NMC, PHEV (d) NMC, HEV

Fig. 7. Results from Monte Carlo simulations with biased current sensor

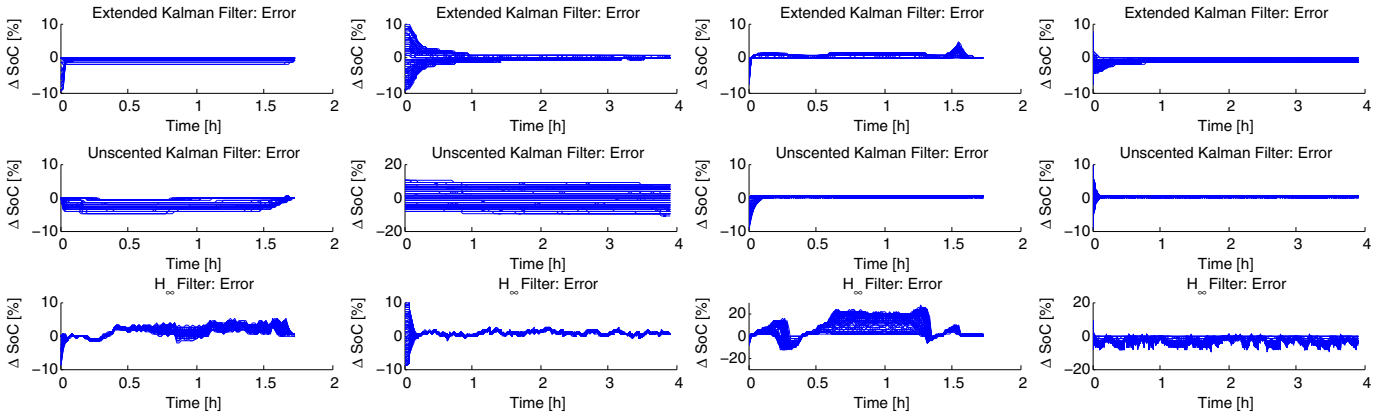

(a) LFP, PHEV (b) LFP, HEV (c) NMC, PHEV (d) NMC, HEV

Fig. 8. Results from Monte Carlo simulations with different variance on the voltage sensor. Note the scaling on the H_∞ filter for NMC and PHEV cycle.

reason it is interesting to see how sensitive the algorithms are to perturbations in parameter tuning.

In this test, two versions of the observers using the same measurement signals and battery models were run. A reference observer using parameters from the procedure in Section 2.3 was compared to an observer where uniformly distributed noise was added to the covariance matrices, Σ_w and Σ_v. For the UKF, also the parameter controlling the distance and weight of the sigma points was changed. For the H_∞ observer, the L matrix was changed in the same manner.

The results are shown in Figure 9, where the differences between the reference observer estimates and the estimates using the perturbed covariances are plotted. The results are similar for all simulations. H_∞ produces the same estimate as long as the requirement of positive definitiveness of (4) is met. For the EKF, it is mainly the convergence rate that is affected by the tuning and the estimation converged for all simulations. The UKF is most sensitive to tuning, and especially the tuning of the parameter controlling the distance and weight of the sigma points. Also note that the UKF estimation diverges for some simulations on the HEV cycle with the LFP battery.

3.5 Comparison

Figure 10 provides an overview of the performance of the different observers. The main findings are:

- For the NMC battery, with strong correlation between OCV and SoC, the UKF outperforms the other observers. On the other hand, when the SoC–OCV relation is flat, the UKF is not a good option since it has convergence problems in several test cases.
- The EKF shows robust behaviour in most cases, except for biased current sensor readings. The impact of the drift is not so obvious in Figure 10, but is best studied in Figure 7.
- The H_∞ observer performs very well considering that there are basically no tuning parameters. However, the estimates for the H_∞ observer are somewhat unpredictable, sometimes giving large errors.

4. CONCLUSIONS

The simulation study reveals significant differences in observer performance that can not be purely attributed to tuning of the observers. Some influence of the tuning can, however, not be ruled out.

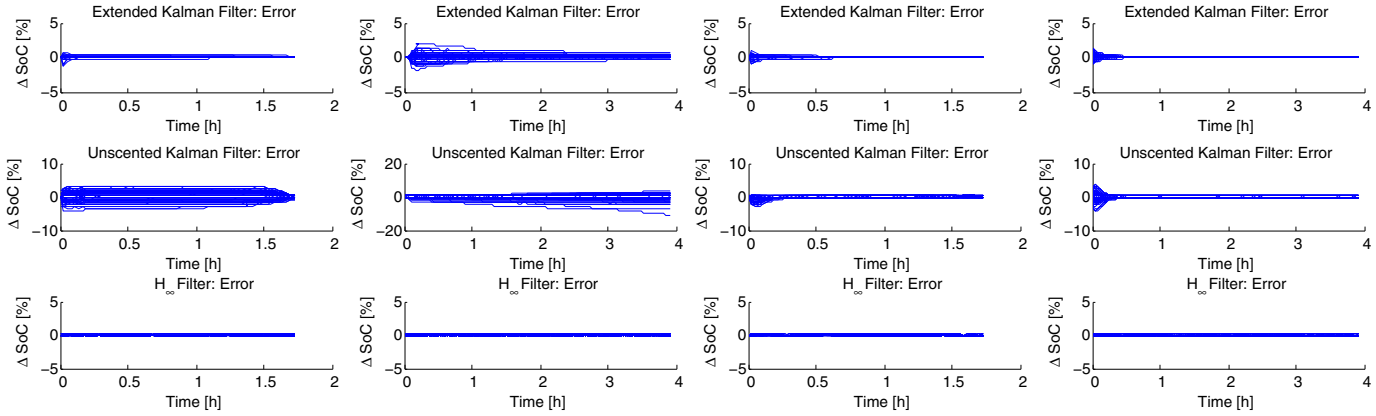

(a) LFP, PHEV (b) LFP, HEV (c) NMC, PHEV (d) NMC, HEV

Fig. 9. Difference between reference observer estimation and estimation using perturbed covariance matrices

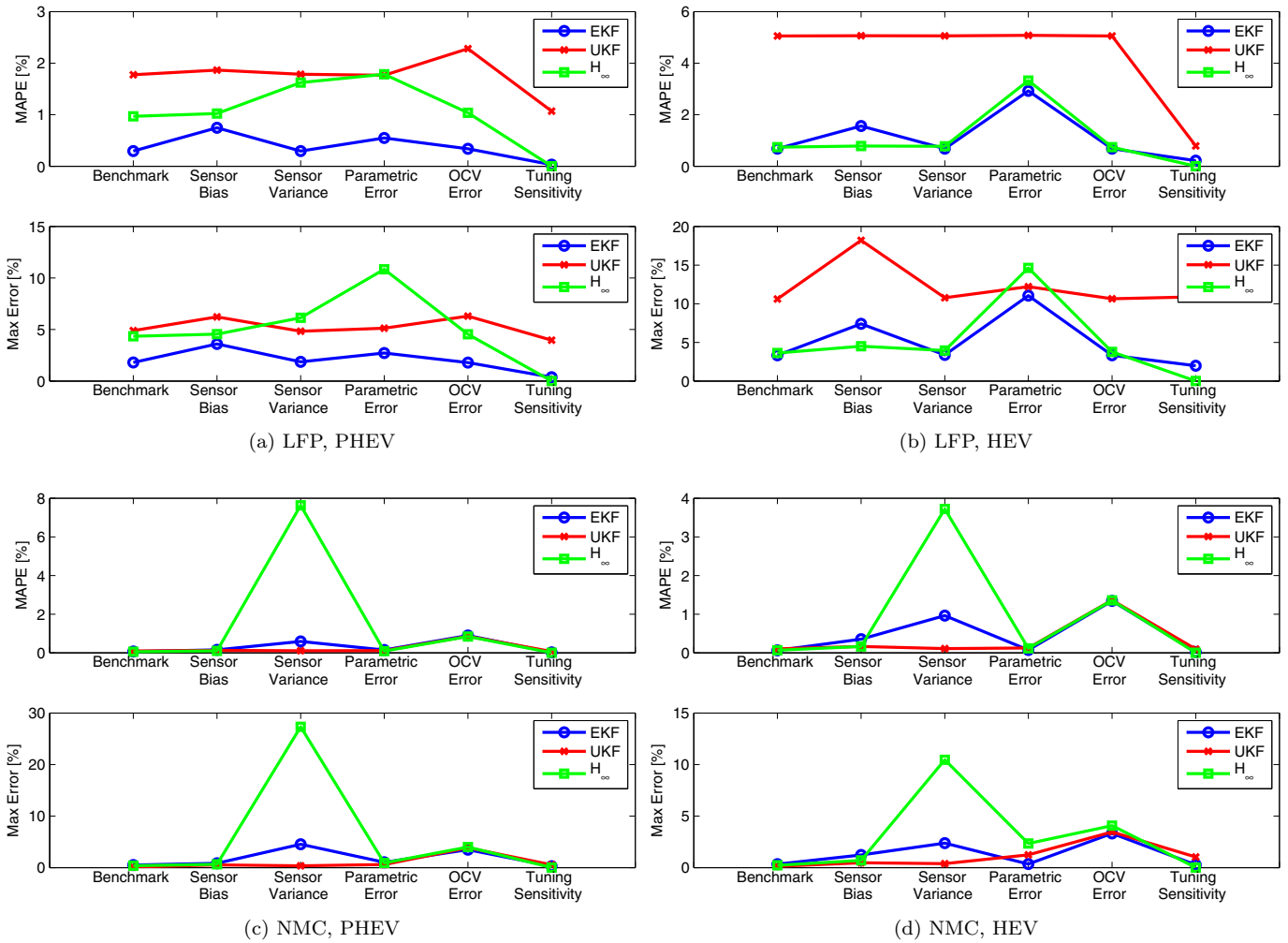

(a) LFP, PHEV (b) LFP, HEV

(c) NMC, PHEV (d) NMC, HEV

Fig. 10. Comparison of the performance in the different cases. Caution should be taken when looking at the absolute values of the estimator performance. It is the relative differences that are in focus here.

The general finding is that when the observability of the system is poor, e.g. on the flat part of OCV curve for the LFP chemistry, it is important that the observer can do controlled Coulomb counting. EKF proved to be best at this task. When the observability is stronger, e.g. for the NMC chemistry, the choice of observer will affect the performance. In this study, UKF performed best for most cases, while H_∞ provided the most consistent estimates with respect to different uncertainties.

The guaranteed robustness bounds of the H_∞ filter are too generous for practical use in SoC estimation. However, the performance of the observer was good in the case of good observability.

REFERENCES

P. Abbeel, A. Coates, M. Montemerlo, A.Y. Ng, and S. Thrun. Discriminative Training of Kalman Filters. *Proc. of Robotics: Science and Systems*, 2005.

X. Chen, W. Shen, Z. Cao, and A. Kapoor. A Comparative Study of Observer Design Techniques for State of Charge Estimation in Electric Vehicles. In *7th IEEE Conference on Industrial Electronics and Applications*, pages 102–107, 2012.

B. Hassibi, A.H. Sayed, and T. Kailath. Linear Estimation in Krein Spaces-Part II: Applications. *IEEE Transactions on Automatic Control*, 41(1):34–49, 1996.

X. Hu, S. Li, and H. Peng. A Comparative Study of Equivalent Circuit Models for Li-Ion Batteries. *Journal of Power Sources*, 198:359–367, 2012.

X. Hu, S. Li, H. Peng, and F. Sun. Robustness analysis of State-of-Charge estimation methods for two types of Li-ion batteries. *Journal of Power Sources*, 217:209–219, 2012.

X. Hu, F. Sun, and Y. Zou. Estimation of State of Charge of a Lithium-Ion Battery Pack for Electric Vehicles Using an Adaptive Luenberger Observer. *Energies*, 3(9):1586–1603, 2010.

I.S. Kim. The Novel State of Charge Estimation Method for Lithium Battery Using Sliding Mode Observer. *Journal of Power Sources*, 163(1):584–590, 2006.

J. Li, J. Klee Barillas, C. Guenther, and M.A. Danzer. A comparative study of state of charge estimation algorithms for LiFePO4 batteries used in electric vehicles. *Journal of Power Sources*, 230:244–250, 2013.

X.R. Li and Z. Zhao. Measures of performance for evaluation of estimators and filters. *Proc. 2001 SPIE Conf. on Signal and Data Processing*, 1–12, 2001.

L. Lu, X. Han, J. Li, J. Hua, and M. Ouyang. A review on the key issues for lithium-ion battery management in electric vehicles. *Journal of Power Sources*, 226:272–288, 2013.

P. Ni. Unscented H_inf filter based simultaneous localization and mapping. In *30th Chinese Control Conference (CCC)*, number 1, pages 3942–3946, 2011.

G. Plett. Extended Kalman filtering for battery management systems of LiPB-based HEV battery packs. Part 1-3. *Journal of Power Sources*, 134(2):252–292, 2004.

G. Plett. Sigma-point Kalman Filtering for Battery Management Systems of LiPB-based HEV Battery Packs. Part 1-2. *Journal of Power Sources*, 161(2):1356–1384, 2006.

J. Seo, M.J. Yu, C.G. Park, and J.G. Lee. An Extended Robust H infinity Filter for Nonlinear Uncertain Systems with Constraints. In *Proceedings of the 44th IEEE Conference on Decision and Control*, pages 1935–1940. Ieee, 2005.

D. Simon. *Optimal State Estimation*. John Wiley & Sons, Ltd, 2006.

G. Welch and G. Bishop. An Introduction to the Kalman Filter. *University of North Carolina at Chapel*, (TR 95-041):1–16, 1995.

J. Yan, G. Xu, H. Qian, and Y. Xu. Robust State of Charge Estimation for Hybrid Electric Vehicles: Framework and Algorithms. *Energies*, 3(10):1654–1672, 2010.